

---

# CFD simulation and PIV measurement of liquid–liquid two-phase flow

Zheng He, Xuan Gu <sup>b</sup>, Xiaoyu Sun <sup>a,\*</sup>, Ju Liu, Binsheng Wang <sup>c</sup>

College of Aerospace and Civil Engineering, Harbin Engineering University, Harbin 150001  
China

<sup>a</sup>sunxiaoyu520634@163.com, <sup>b</sup>guxuan@hrbeu.edu.cn, <sup>c</sup>wangbinsheng@hrbeu.edu.cn

---

## Abstract

Microemulsion systems may enable innovative and highly efficient synthesis paths for the chemical industry. When expensive catalysts are involved in the process, an efficient separation of products together with an extremely low catalyst leaching are of utmost importance. In order to optimize the separation process and improve the settler design, a thorough understanding of droplet-droplet interactions is required. In this work, computational fluid dynamics (CFD) has been used to study the multiphase flow in a horizontal settler using the Eulerian two-fluid framework. Droplet coalescence, which is the most important physical phenomenon in gravity-driven separation, has been modeled using a spatially inhomogeneous buoyancy-based kernel, and the resulting population balance equation has been solved using the quadrature-based method of moments (QMOM). After calibrating the model parameters using selected experiments, a very good description of the observed separation is obtained, opening the door for process understanding and optimization.

## Keywords

Index Terms—Gravity separation; Microemulsion; Coalescer; Population balance; Method of moments; Computational fluid dynamics

---

## 1. Introduction

The separation of multiphase systems is important for various industrial applications, e.g., isolation of products or catalyst recovery after a chemical reaction. Of the many possible techniques, the use of a gravity settler is often preferred due to its simplicity and low costs [1-3]. Separation of liquid-liquid mixtures in a gravity settler is mainly driven by coalescence of liquid droplets of the dispersed phase. The process of coalescence leads to the formation of bigger drops, which then readily separate from the continuous phase under the influence of gravity.

In order to model droplet-droplet interactions, PBEs have been solved using quadrature method of moments (QMOM) [4]. This approach results in low computational cost and relatively high accuracy as compared to other methods[5]. However, the efficacy of these methods depends also on the relative magnitude and the number of moments chosen to describe the droplet distribution, as difficulties may arise in the solution algorithm if the moments vary over a large range. While the choice of a higher number of moments usually increases the accuracy of the solution, it also increases the associated computational costs. Moreover, such a choice, when coupled with the use of a higher-order spatial discretization scheme, may also lead to numerical instabilities due to the presence of unrealizable nodes [6]. A description of the evolution of the droplet-size distribution using two quadrature nodes is usually enough to achieve an acceptable degree of accuracy [5]. For this reason, the solution in the present work has been computed using four lower-order moments of the droplet-size distribution. A

buoyancy-driven coalescence kernel based on the one proposed by Prince and Blanch[7] has been implemented with appropriate modifications to account for the effect of the porous medium on separation, as described later. The primary reason for the choice of this kernel was its simplicity, as only one fitting parameter is required. At least three parameters are needed in the kernel proposed by Grimes[8], which will also be considered and might become even more important for later studies. First simulation results with the buoyancy-driven coalescence kernel already show a good agreement with experimental data, as discussed later. The final objective of the present study is to improve our knowledge concerning separation of micellar multiphase systems to develop improved operational strategies.

## 2. Simulation

Fig. 1 shows a three-dimensional model of the horizontal settler with an internal diameter of 56 mm. The settler has two outlets – a product stream at the top and a recycle stream at the bottom, each with an inner diameter of 7 mm. The coalescer is placed towards the inlet side and contains a central solid core (non-porous zone) of diameter 50 mm to redirect fluid flow towards the outer edges. The geometry has been meshed using an O-grid structured mesh with 160,000 cells. This number of cells is needed to ensure grid-independency, as found in a preliminary study. The values of minimum orthogonal quality, maximum orthogonal skew and maximum aspect ratio associated with this mesh are 0.29, 0.72, and 19.2, respectively, denoting a good quality.

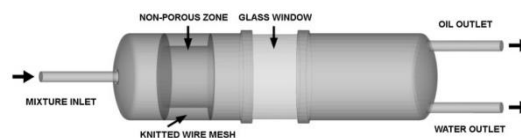


Fig. 1 Geometry of the horizontal separator.

Simulations have been performed for the separation of an educt system composed of 1-dodecene, diethyleneglycolbutylether (C4E2), and water. Reaction is neglected in this study, since first experiments were performed with educts, before initiating the reaction. In such a system, the three-phase region persists in a temperature range between 80 °C and at least 96 °C, with the organic phase being the continuous phase in which the aqueous and bicontinuous phases are dispersed[9]. In order to operate the settler in a continuous mode, a narrow temperature window around the optimum separation temperature needs to be maintained. The mass fraction of surfactant in the system influences this optimum separation temperature, thereby causing the temperature window to shift [10]. The surfactant concentration also has a direct influence on the volume fraction of the bicontinuous phase. However, a very small influence of the surfactant concentration on the physical properties of the phases was reported [9].

## 3. Results and discussion

The best results, obtained for the parameters listed previously, lead to a very good agreement between numerical predictions and experimental observations, as illustrated in Fig. 2. This figure shows in color the evolution of the volume fraction of the bicontinuous phase vs. time in the computation. Originally, the bicontinuous phase is not present; over more than 60 s, phase separation occurs and a clear region with pure bicontinuous phase (volume fraction  $\approx 1$ ) appears between the organic and the aqueous phase. The two black lines show the phase boundaries observed in the experiments.

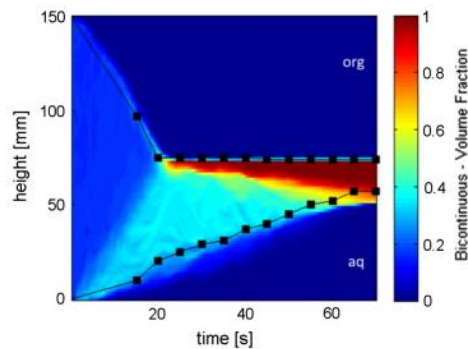


Fig. 2 History of phase separation in time, starting from homogeneous conditions.

Experimentally-measured phase boundaries (black lines) and computed volume fraction of the bicontinuous phase (color plot). (For interpretation of the references to color in this figure legend, the reader is referred to the web version of this article.)

In order to study the effect of coalescence kernels on separation, first simulations were performed without accounting for the porous medium. Next, the buoyancy-driven coalescence model described previously was implemented. Finally, a simplified form of the coalescence kernel proposed by Grimes [8] was also tested under the same conditions, assuming a constant surfactant concentration throughout the settler. Fig. 3 compares the obtained volume fraction of the bicontinuous phase in the settler at the end of 500 s flow time, using the three models. This duration leads to converged results, as the residence time is roughly 100 s under the chosen conditions. As the bicontinuous phase lies due to its density between the upper (organic) and lower (aqueous) phase layers, showing its volume fraction is the most convenient way of representing separation in the three-phase system. The white rectangle in these figures represents the location of the central solid insert.

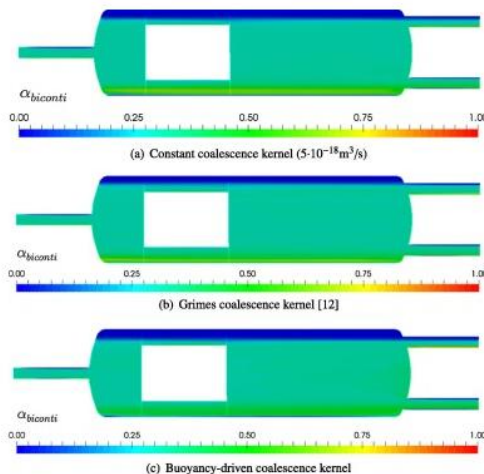


Fig. 3 Comparison of volume fractions of the bicontinuous phase using different coalescence kernels at  $t=500$  s. The Grimes kernel (Grimes, 2012) implemented in this simulation assumes a constant temperature and phase composition throughout the settler (color plot).

Next, simulations including the energy transport equation were performed to obtain a realistic temperature field. Fig. 4 shows again the volume fraction of the bicontinuous phase at the end of 500 s flow time for the model of Grimes, in which temperature impacts the coalescence kernel. Comparing Fig. 3 ; Fig. 4, there is a marked change in the results, which now correspond to a much better separation of the upper organic layer, as well as of the aqueous and bicontinuous phases, with a low organic phase content in the lower outlet.

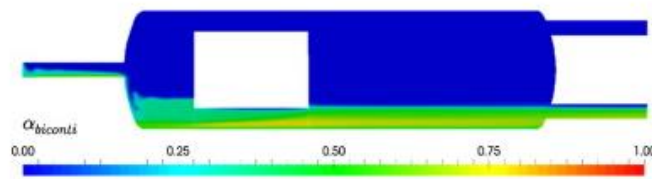


Fig. 4 Volume fraction of the bicontinuous phase using Grimes coalescence kernel (Grimes, 2012) at  $t=500$  s. The Grimes' kernel implemented in this simulation considers the effect of non-homogeneous temperature on coalescence, while the surfactant concentration has been assumed to be constant in both space and time (color plot).

Müller et al.[10] have determined that a temperature range of 4 K applies for an optimal continuous operation of the settler. This optimum temperature range shifts depending on the amount of surfactant present in the system. Fig. 5(a) shows the temperature field in a vertical cut through the center of the settler, and compares it to experimentally measured values. Fig. 5(b) shows the temperature in the settler obtained by CFD and also marks (as a black line) the location of the previous comparison. The observed differences can be attributed to the fact that the phase properties have been considered to be independent of temperature in the simulation. Additionally, a large-scale recirculation is observed in this region. Minor changes in the position of this recirculation strongly impact the comparison along the black line. Keeping this in mind, an acceptable agreement with the experimental values is found, with a good prediction of the general trend and of both minimum and maximum values.

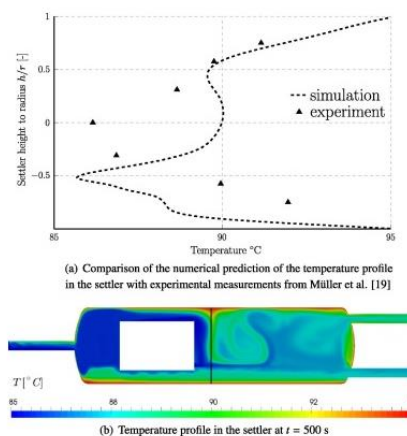


Fig. 5 Temperature field in the settler. In (a), a height-to-radius ratio of 0 indicates the central longitudinal plane through the settler, with negative values indicating the lower half of the settler. Gravity is from bottom to top. The place for which this comparison has been made is shown in (b) as a black line (color plot).

Fig. 6(a) shows the variation of the gauge pressure in the settler along the streamline shown in Fig. 6(b) as a white line. It can be seen that gravity is dominating the pressure evolution in the settler. The coalescer offers significant resistance to the flow, with only small pressure changes outside of the wire mesh.

As expected, the effect of the porous medium on separation was most pronounced in the case of the buoyancy-driven kernel, as shown later in Fig. 8(a). This kernel now predicts a noticeably better separation of all phases. Because this model is based on the relative velocities of approaching droplets, which are directly affected by the inclusion of the additional momentum exchange term, such an effect is to be expected. Fig. 7 shows the velocity profile of the continuous phase in the settler at a flow time of 500 s. The observed recirculation zones in the settler due to the influence of the coalescer impact residence time, collision frequency and, in turn, separation. These recirculation zones also have a large impact on the temperature profile, again affecting separation when considering Grimes' kernel.

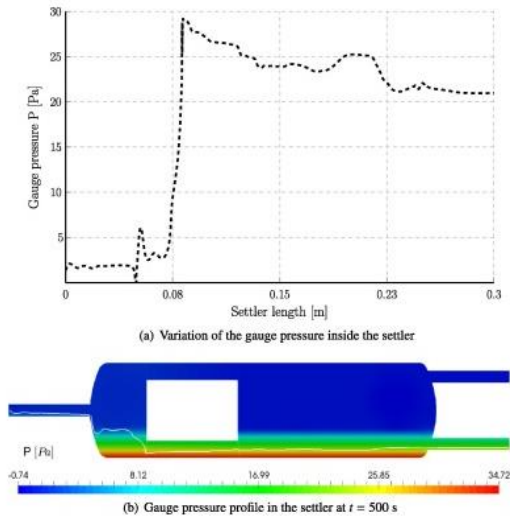


Fig. 6 Pressure field in the settler. In (a), the change of pressure is mapped along a streamline shown in (b) as a white line (color plot).

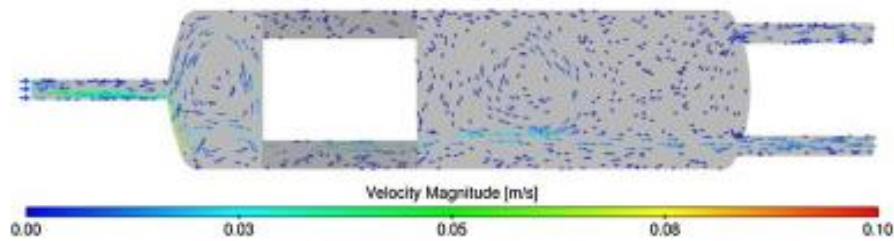


Fig. 7 Velocity profile of the continuous phase in the settler at  $t=500$  s (color plot).

The result of this modification, as expected, is a further enhancement in the prediction of phase separation. Fig. 8(b) shows again the volume fraction of the bicontinuous phase in the settler at the end of the simulation. By comparison with Fig. 8(a), it is clear that the local change in collision efficiency induces large modifications in the results.

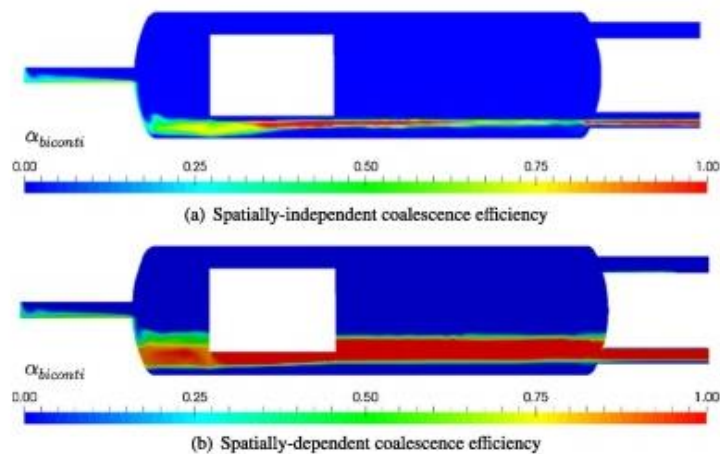


Fig. 8 Volume fraction of the bicontinuous phase at  $t=500$  s using the buoyancy-driven coalescence kernel: (a) with coalescence efficiency given everywhere by Eq. (14); (b) with coalescence efficiency locally increased to 1 within the coalescer (color plot).

A comparison of these results with those obtained from experiments is presented in Fig. 9. It shows the time-evolution of the organic phase volume fraction in the bottom outlet of the settler.

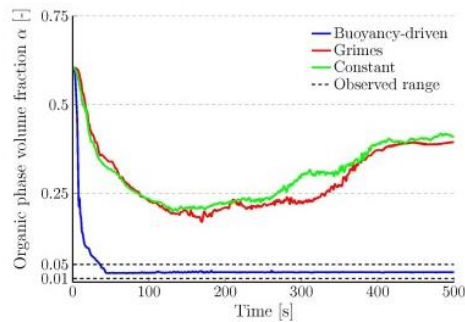


Fig. 9 Time-evolution of organic phase volume fraction at the bottom outlet of the settler. The two horizontal dashed lines represent the upper and lower bounds of the organic phase volume fraction observed experimentally during the measurement campaign. The time axis is only associated to the three computational results shown as solid lines (color plot)

#### 4. Conclusion

In this work, the separation process in a horizontal settler has been simulated using a two-fluid Eulerian approach. Population balance equations for the description of droplet-droplet interactions have been solved using the QMOM approach. Two quadrature nodes have been used in the solution of the resulting moment transport equations. A total of three coalescence kernels have been tested in the present study – a constant kernel, a buoyancy-driven kernel, and Grimes' kernel [8]. As expected, the constant kernel was not able to reproduce the complexity of the process. It was found that the buoyancy-driven coalescence kernel was most appropriate for the description of the present system. This model assumes that coalescence is driven by gentle collisions, and the frequency of binary collisions depends on the sizes of the approaching droplets. The efficiency of coalescence is assumed to be a function of the relative approach velocity of colliding droplets. Effects of the employed coalescer on fluid flow as well as on coalescence efficiency have been included in the model, by considering the coalescer as a porous zone and increasing the efficiency term within this porous region. Since the porous zone consists of a very fine wire mesh, the efficiency in this zone is assumed to be unity. The critical velocity appearing as a model constant was set by fitting the observed results concerning separation of the same system in a beaker. Following experimental observations, the Sauter mean diameter of the bicontinuous phase was related to that of the aqueous phase with the help of a second, experimentally-determined parameter. As observed experimentally, a significant influence of the coalescer was found concerning flow velocity as well as separation. Finally, the simulation results show an excellent agreement with experimental data from a continuous mini-plant operation campaign.

However, a direct application of the employed coalescence kernel to a wide range of operating conditions is limited. A generally-valid coalescence model should take into account the effects of local surfactant concentration and temperature. In this regard, the Grimes' kernel is a promising alternative. Even though it failed to make correct predictions in the present study when neglecting changes in the local surfactant concentration, it will be considered further in future work. Finally, describing separately the two disperse populations by separate QMOM models is currently being implemented.

#### Acknowledgements

This work is part of the Collaborative Research Center "Integrated Chemical Processes in Liquid Multiphase Systems" (Subproject B8) coordinated by the Technische Universität Berlin. Financial support by the German Research Foundation (Deutsche Forschungsgemeinschaft, DFG) is gratefully acknowledged (TRR63). Furthermore, the authors gratefully acknowledge the help and support provided by Gábor Janiga in the setup and analysis of CFD simulations. A special thank goes to Yongfei Yang for generating the 3D settler geometry. Also, we acknowledge the support of Rhodius

GmbH with knitted wire meshes for operating the mini-plant, as well as for providing all needed information.

This work is supported by the National Natural Science Foundation of China (No. 11602066) and the National Science Foundation of Heilongjiang Province of China (QC2015058 and 42400621-1-15047), the Fundamental Research Funds for the Central Universities.

## References

- [1] M. Ruiz, R. “Padilla Separation of liquid-liquid dispersions in a deep-layer gravity settler. 2: Mathematical modeling of the settler Hydrometallurgy,” 42 (2) (1996), pp. 281–291
- [2] R. Padilla, M. Ruiz, W. “Trujillo Separation of liquid-liquid dispersions in deep-layer gravity settler.” 1: Experimental study of the separation process Hydrometallurgy, 42 (2) (1996), pp. 267–279.
- [3] S.K. Panda, K. Singh, K. Shenoy, V.V. “Buwa Numerical simulations of liquid-liquid flow in a continuous gravity settler using OpenFOAM and experimental verification Chem. Eng. J. ” 310 (Part 1) (2017), pp. 120–133.
- [4] R. McGraw .“Description of aerosol dynamics by the quadrature method of moments Aerosol Sci. Technol, ”27 (2) (1997), pp. 255–265.
- [5] D.L. Marchisio, R.D. Vigil, R.O. “Fox Implementation of the quadrature method of moments in CFD codes for aggregation/breakage problems Chem. ”Eng. Sci., 58 (15) (2003), pp. 3337–3351.
- [6] L. Mazzei, D.L. Marchisio, P. Lettieri. “New quadrature-based moment method for the mixing of inert polydisperse fluidized powders in commercial CFD codes AIChE J,”58 (10) (2012), pp. 3054–3069.
- [7] M.J. Prince, H.W. “Blanch Bubble coalescence and break-up in air-sparged bubble columns AIChE J,” 36 (10) (1990), pp. 1485–1499.
- [8] B.A. Grimes. “Population balance model for batch gravity separation of crude oil and water emulsions. ”Part I: Model formulation J. Dispersion Sci. Technol., 33 (4) (2012), pp. 578–590
- [9] L. Hohl, J. Schulz, N. Paul, M. Kraume. “Analysis of physical properties, dispersion conditions and drop size distributions in complex liquid/liquid systems Chem”. Eng. Res. Des., 108 (2016), pp. 210–216.
- [10] D. Müller, E. Esche, T. Pogrzeba, M. Illner, F. Leube, R. Schomäcker, G. Wozny. “Systematic phase separation analysis of surfactant-containing systems for multiphase settler design,” Ind. Eng. Chem. Res., 54 (12) (2015), pp. 3205–3217